PERGAMON

Journal of Structural Geology 22 (2000) 735–756

JOURNAL OF STRUCTURAL GEOLOGY

www.elsevier.nl/locate/jstrugeo

The formation of an orocline by multiphase deformation: a paleomagnetic investigation of the Cantabria–Asturias Arc (northern Spain)

Arlo B. Weil*, R. Van der Voo, B.A. van der Pluijm, J.M. Parés

Department of Geological Sciences, University of Michigan, Ann Arbor, MI 48109, USA

Received 22 February 1999; accepted 13 December 1999

Abstract

The Variscan orogeny in the Cantabria–Asturias Arc (CAA) of northern Spain represents a multiphase deformation history associated with Pangea's amalgamation. To determine the timing and kinematic history of deformation, a paleomagnetic investigation was carried out on Devonian limestones in three structural domains of the CAA's hinge zone.

Two characteristic remagnetizations in the CAA are distinguished: an Early Permian (B) component that postdates initial Westphalian–Stephanian aged folding (F_1 and F_2), and a Late Carboniferous (C) component that postdates F_1 deformation. Both the B and C magnetizations experienced a later F_3 folding phase. The kinematics and geometry of post-magnetization deformation are determined by bringing measured magnetic directions into agreement with reference directions. These structural corrections also allow separation of deformation events in time. We conclude that generally east–west-trending, but variably plunging, fold axes characterize F_3 folding in the hinge zone of the CAA. This post-magnetization deformation involved significant amounts of tilting and (sub)vertical axis rotation, which together produced clockwise rotation in the north of the arc and counterclockwise rotation in the south of the arc, to form the horseshoe-shaped orocline that is observed today. F_3 fold axes change from near-vertical to moderately inclined between and within structural domains, due to the structural fabric imposed by F_1 and F_2. Based on calculated F_3 fold properties, we can reconstruct pre-existing F_1 and F_2 structural geometries of the hinge zones. This analysis shows that F_1 and F_2 structures are the result of Late Carboniferous deformation, as part of the same east–west but temporally discrete compression regimes. On the other hand, F_3 is controlled by Permian, north–south compression (in present-day coordinates).

1. Introduction

The Cantabria–Asturias Arc (CAA) is the foreland fold-and-thrust belt of northern Iberia's Variscan orogen and makes up the core of the larger Ibero-Armorican Arc (Fig. 1). The CAA is an unusual orogenic belt that curves 180°, with a geometry that is concave towards the foreland; i.e. folds and thrusts verge toward the core of the arc. The CAA is generally considered to be a thin-skinned fold-and-thrust belt that is tectonically related to the convergence between Gondwana and Laurussia during the Late Paleozoic amalgamation of Pangea (Ries and Shackleton, 1976; Pérez-Estaún et al., 1988). Following Carey's (1955) orocline hypothesis, a number of models have been suggested for the formation of the CAA. Matte and Ribeiro (1975) suggested that the curvature is due to the displacement of a 'Cantabria microplate' westward, whereas Ries and Shackleton (1976) proposed that the orocline formed by late Variscan north–south compression that produced a counterclockwise rotation of central and southern Iberia relative to Brittany. Pérez-Estaún et al. (1988) hypothesized a continuous deformation phase of progressive rotational thrust displacements propagating from west to east. Previously, paleomagnetism has been used to characterize the arc's

* Corresponding author.
E-mail address: abweil@umunich.edu (A.B. Weil).

0191-8141/00/$ - see front matter
PII: S0191-8141(99)00188-1

history and to demonstrate that at least some of the arc's curvature is of secondary nature (Bonhommet et al., 1981; Perroud, 1982, 1983, 1984, 1985; Hirt et al., 1992; Stewart, 1995; Parés et al., 1994; Van der Voo et al., 1997). However, considerable debate remains about the kinematic development of the CAA and the timing of the region's deformation history. In this paper we will use paleomagnetism as a discriminating tool for the characterization of fold generations and their timing, and propose an internally consistent deformation history for the arc.

Early structural analyses by de Sitter (1965), Julivert (1971) and Julivert and Marcos (1973) documented two main phases of Variscan deformation in the CAA. The early phase is an east–west shortening event (in present-day coordinates) resulting in thrust initiation and 'longitudinal' folds. These folds are related to thrust emplacement and are characterized by horizontal fold axes and steep axial surfaces that parallel the curvature of the arc. The detailed morphology and geometry of the folds are related to a ramp-and-flat thrust system that dominates the CAA. The synclines, developed over thrust-flats, are usually open with relatively flat bottoms, whereas the anticlines, developed in the hanging wall over thrust-ramps, are often tight and sometimes breached into fault-propagation folds (Pérez-Estaún et al., 1988). This early deformation phase is temporally divided into two episodes by at least one (brief) hiatus at the Stephanian–Westphalian boundary (ca. 296 Ma) (Julivert, 1971), which we attribute to a change in the kinematics of folding. Thus, the first phase of folding (longitudinal north–south-trending folds) is herein divided into two generations, F_1 and F_2. F_1 folding characterizes the main stage of thrusting and longitudinal fold initiation, whereas F_2 resulted in further shortening and tightening of F_1 folds with an added component of (sub)vertical-axis rotation. The second phase, which is associated with the arc's ultimate tightening (represented herein as F_3), is characterized by a 'radial' set of folds commonly with steep fold axes (Julivert, 1971). However, the 'radial' geometry of F_3 only describes the present-day

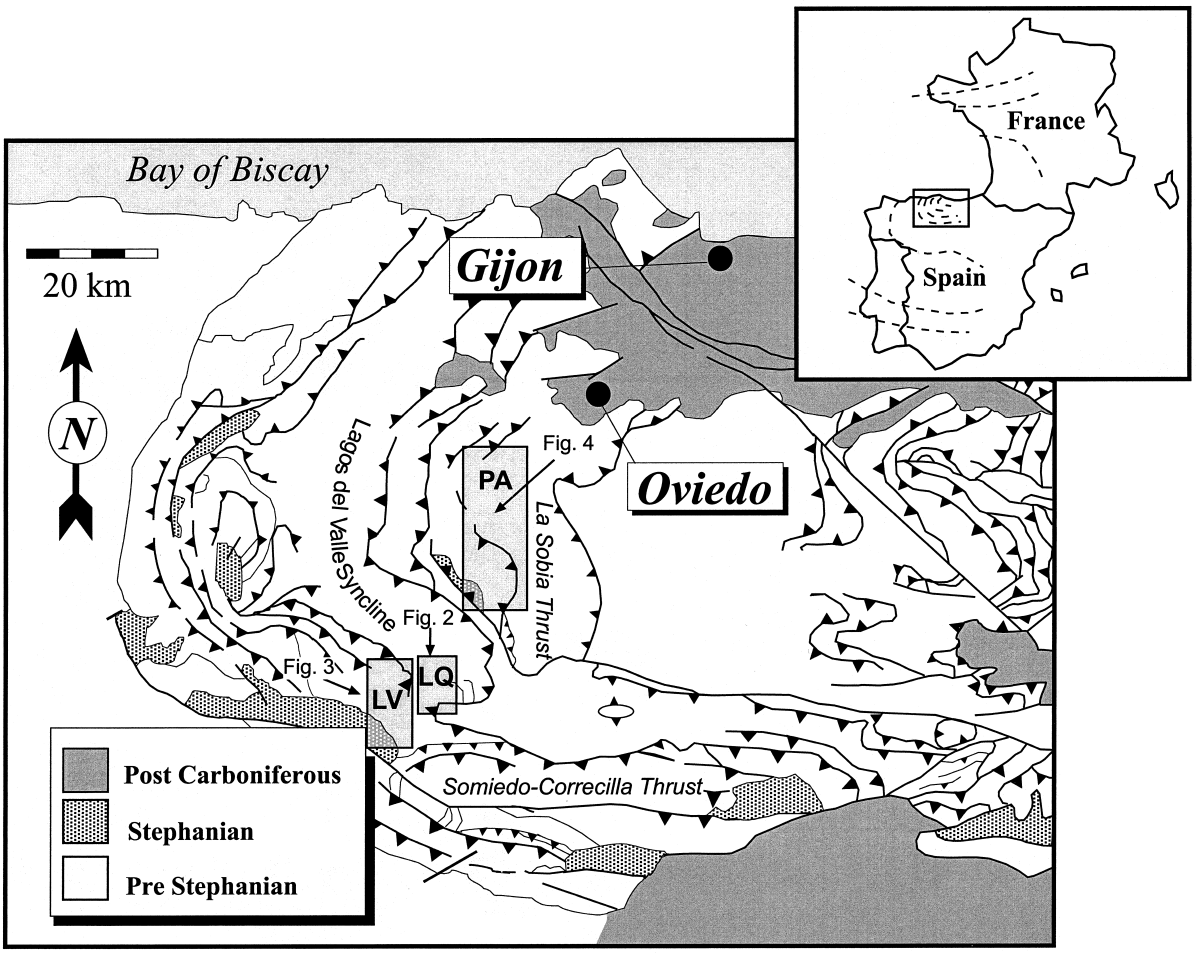

Fig. 1. Simplified structural map of the Cantabria–Asturias Arc, northern Spain. Highlighted in grey boxes are the three structural domains studied (LV = La Vega de los Viejos Syncline, LQ = La Queta Syncline, PA = Proza Anticline). Also shown is the Lagos del Valle Syncline studied by Van der Voo et al. (1997).

configuration of the folds, and says little about the kinematics of the event that produced them. Consequently, the nature of F_3 folding has remained speculative. Several models have been proposed for the manifestation of F_3 fold geometries within the CAA. Aller and Gallastegui (1995) proposed that F_3 has (sub)horizontal fold axes, whereas Stewart (1995) and Ries et al. (1980) argued for steep F_3 axes. Julivert and Marcos (1973) and Bonhommet et al. (1981) proposed vertical axis rotation, and Van der Voo et al. (1997) argued for F_3 being (sub)vertical with local tilting. Because these studies derive their observations from different regions of the CAA, they may all be correct if F_3 fold axes vary from domain to domain. Alternatively, these orientations may reflect different fold generations. Thus, we need to characterize F_3 on the regional scale in order to constrain the kinematics and development of the CAA's late history.

Recent paleomagnetic work (Parés et al., 1994; Stewart, 1995; Van der Voo et al., 1997) has shown that the magnetizations of all the pre-Variscan, CAA Paleozoic rocks are secondary in origin. Similar to Van der Voo et al. (1997), we recognize three separate magnetic components: an A-component that is similar to Spain's present-day field, an Early Permian B-component that has shallow inclinations and postdates initial F_1 and F_2 folding, and a Late Carboniferous C-component that is acquired between F_1 and F_2 folding. Both the B and C magnetic components experienced the later F_3 deformation.

This paper describes a detailed paleomagnetic study of three individual structural domains within the hinge zone of the CAA to unravel the geometry and timing of Variscan deformation and determine regional structural characteristics. These three domains complement the study Van der Voo et al. (1997) made of the Lagos del Valle Syncline (Fig. 1). The hinge zone of the arc was chosen for this study because of the high angle between axial surfaces of F_1/F_2 and F_3. The deformation history of each structural domain was analyzed using the inherent property of paleomagnetic vectors to record rotations and tilts subsequent to magnetization acquisition. The results from our analysis are used to erect a model for the kinematics of oroclinal bending in the CAA and the temporal and geometric relationship between the different folding phases in the Variscan orogen of northern Spain.

2. Geologic setting

The Paleozoic rocks of the Ibero-Armorican Arc originated in an epicontinental sea that is probably related to the western proto-Tethyan or Iapetus-bordering shelf (Nairn and Smithwick, 1976; Martinez-Garcia, 1991). The Devonian strata of this area represent a series of reef facies that change from northeast to southwest (in present-day coordinates): back barrier, barrier and fore-barrier paleo-reef environments (Reijers, 1980; Pérez-Estaún et al., 1990). The distributions of these facies, characterized by stratigraphic thickening to the west, represent a marker for the ancient central-Iberian coastline (De Sitter, 1965).

The two stratigraphic units sampled in this study, the Santa Lucia and Portilla formations, crop out extensively. These two formations, characterized as Gedinnian to Frasnian-aged reefoid limestone (Reijers, 1985), show little or no penetrative cleavage and appear to have only undergone a small amount of internal deformation.

After a relatively quiescent tectonic period of sedimentation and reef propagation, an overall compressive regime began to dominate in Western Europe in the Late Devonian. This change to a period of active tectonism was the result of northward and westward movement of the Iberia microcontinent, relative to Gondwana, and its eventual collision with Western Europe, Laurentia and Gondwana in the late Carboniferous (Ziegler, 1982). This tectonic phase represents the main pulse of Paleozoic European continent-scale

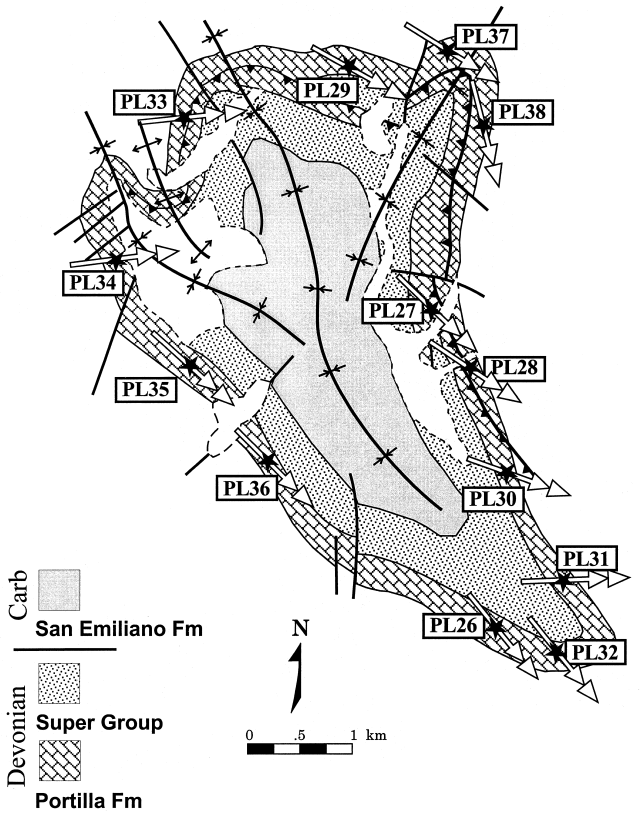

Fig. 2. A schematic geologic map of the La Queta Syncline with in-situ magnetic declinations depicted as white arrows. Notice the more uniform declinations in the southern half of the structure (below sites PL35 and PL38) compared to the much more complicated pattern in the northern half.

deformation, the Variscan orogeny, which caused the Cantabria region of northern Spain to undergo foreland style deformation and develop ultimately into the core of Western Europe's Ibero-Armorican Arc (Matte, 1991; Bachtadse and Van der Voo, 1986). Reviews of the stratigraphy, lithology, basin history, and general structural and tectonic history of the region can be found elsewhere (e.g. Julivert, 1971; Julivert and Marcos, 1973; Reijers, 1980, 1985; Pérez-Estaún et al., 1988).

2.1. Structural domains sampled for this study

The Santa Lucia and Portilla formations were sampled in three structural domains: the La Queta and La Vega de los Viejos Synclines, and the Proza Anticline. The La Queta and La Vega de los Viejos domains are splays in the larger Somiedo-Correcilla thrust unit (Fig. 1). The Proza domain is part of the La Sobia thrust unit, which is more internal to the arc (Fig. 1). These two units are considered the most significant allochthonous thrust sheets in the fold–thrust province of the CAA (Julivert, 1971).

The La Queta domain (Fig. 2) contains a doubly plunging, NNW–SSE-trending syncline that has undergone refolding in both its northern and southern regions. It is positioned in the outer southern bend zone of the CAA in an en échelon arrangement with the Lagos del Valle and La Vega de los Viejos Synclines (Fig. 1; Julivert and Marcos, 1973; see also Van der Voo et al., 1997). The La Queta Syncline is bounded on its east and west by tightly folded

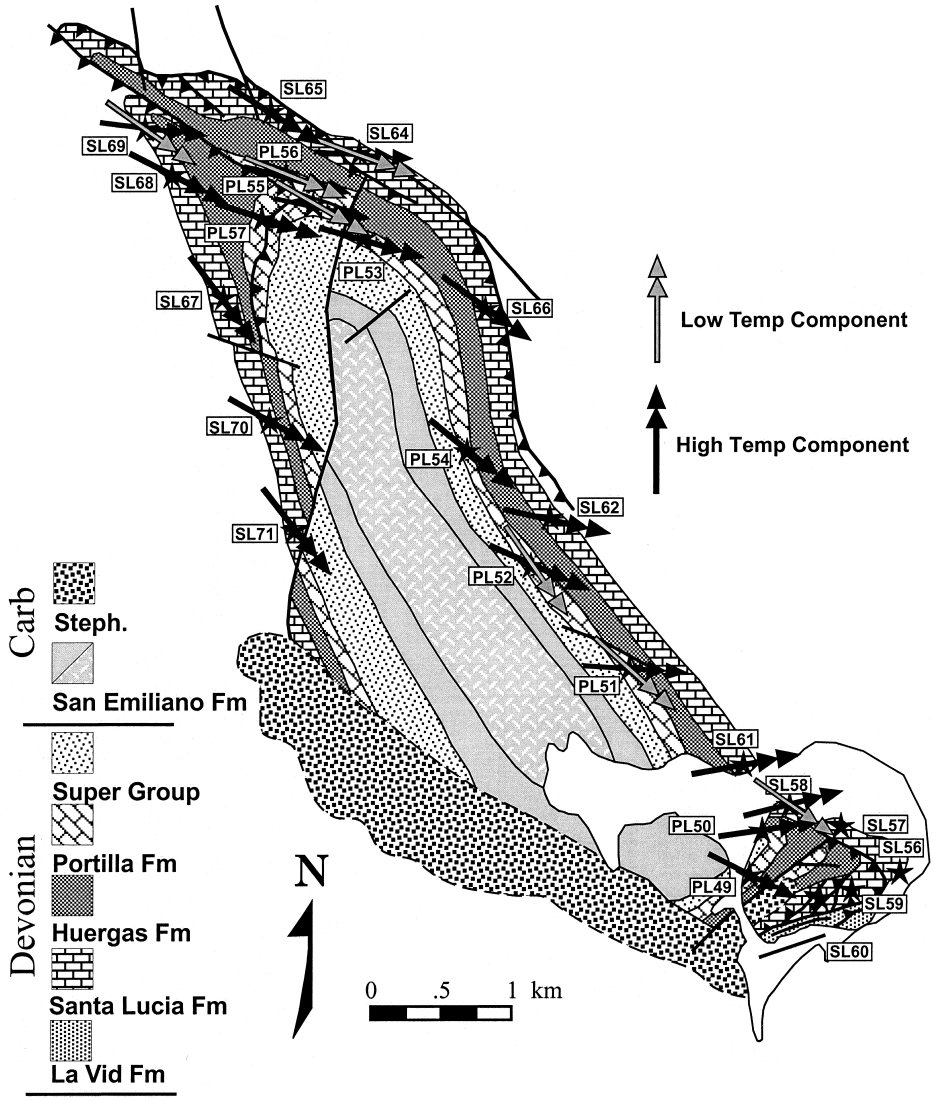

Fig. 3. A schematic geologic map of the La Vega de los Viejos Syncline with in-situ magnetic declinations depicted as black arrows for high temperature components and gray for low temperature components. Notice the strong correlation of strike and declination, as well as the highly faulted southern section.

anticlines with nearly vertical limbs. The attitudes of both synclinal limbs show a component of (sub)vertical axis rotation in their sinuous outcrop patterns, which was attributed by Julivert and Marcos (1973) to interference of multiple fold generations; a first fold generation with vertical axial surfaces and horizontal fold axes, and a second generation with axial surfaces orthogonal to that of the first generation.

The more westerly La Vega de los Viejos Syncline has a NW–SE axial trend with both limbs showing a component of (sub)vertical axis rotation similar in magnitude and direction to the La Queta Syncline (Fig. 3). The entire structure is cut by a large right-lateral oblique-slip fault, and cut locally by bedding-parallel thrusts. The southern edge of the Viejos Syncline is heavily faulted by imbricated thrusts and strike-slip faults due to its proximity to the more faulted southern Correcilla Unit.

Directly to the east of the Lagos del Valle Syncline (Van der Voo et al., 1997) in the central bend zone of the CAA lies the Proza Anticline (Fig. 1). The Proza Anticline is an overthrust structure that dies out to the north into an anticline (Fig. 4). Such fault–fold couplets (e.g. Alvarez-Marrón, 1995; Stewart, 1995) are typically associated with space problems and shortening in CAA overthrusts, as well as other curved fold-and-thrust belts (Julivert and Arboleya, 1984). Cantabrian overthrusts, such as the Proza Anticline, often have complex internal structures and usually appear in multiple stacks that produce stratigraphic repetition

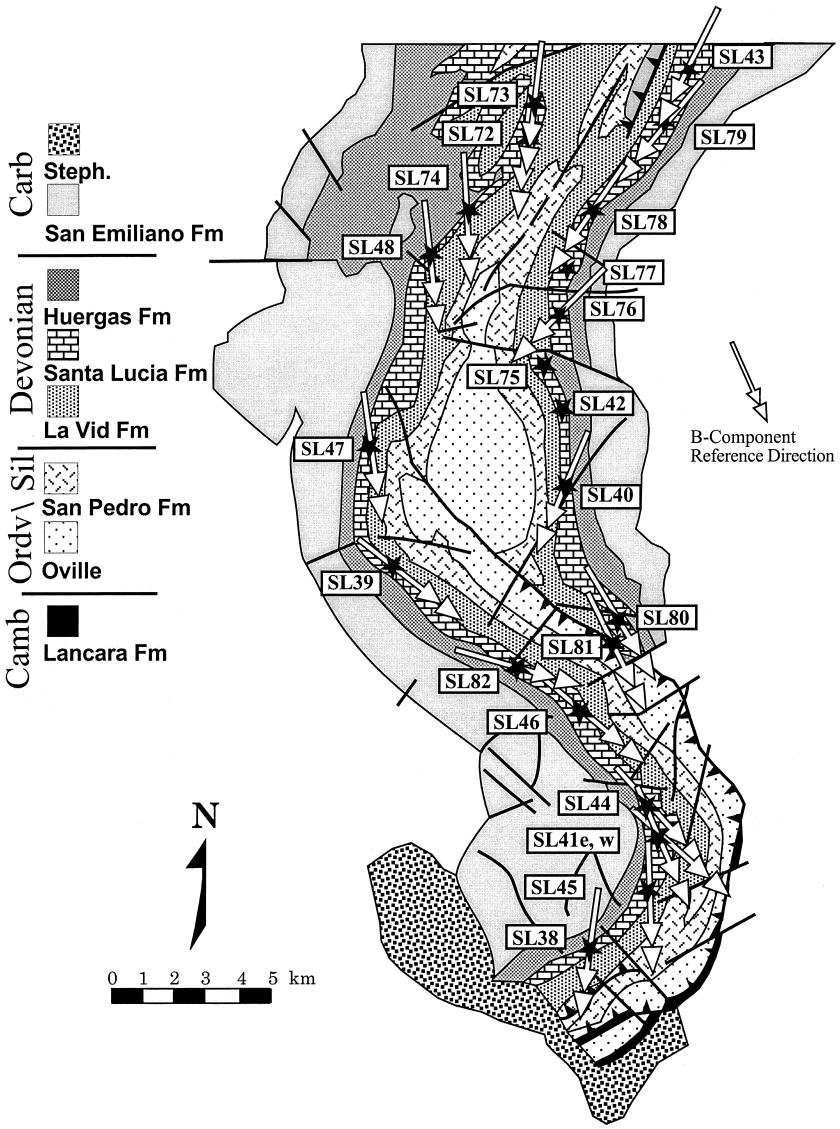

Fig. 4. A schematic geologic map of the Proza Anticline with in-situ magnetic declinations shown as white arrows and site locations in black stars. Notice the strong correlation of strike and declination, especially in the southern bend zone. Reference B magnetization is shown for relative comparison of individual site rotations.

and thickening (Bonhommet et al., 1981). The schematic geologic map in Fig. 4 shows the eastern limb of the Proza anticline truncated by the western limb in response to an eastward propagating thrust. The anticline itself has a small interlimb angle of 30–45°, and a hinge line that is oblique to the direction of thrust movement (Julivert and Arboleya, 1984). Julivert and Arboleya (1984) proposed that the Proza Anticline is the result of thrust emplacement by rotational motion centered at the northern fault terminus. Such a kinematic scenario would require that the thrust sheet be progressively curved as it was emplaced, rather than moving as a rigid plate. Thus, according to this model, the tightening of the structure and its curvature would be contemporaneous with thrust emplacement and not the result of multiple deformation events. This view can be tested with detailed paleomagnetic data.

3. Sampling and experimental methods

Approximately 500 cores were collected in the summers of 1996 and 1997 at 22 sites in the Portilla Formation and 38 sites in the Santa Lucia Formation. Site locations were distributed throughout all three structural domains and severe outcrop weathering and highly faulted areas were avoided where possible. Oriented samples were collected in the field using a portable drill and a magnetic compass. Bedding directions and shear-sense indicators were measured in the field using a magnetic compass.

On average, from seven to ten standard 2.54-cm-diameter paleomagnetic specimens from each site were progressively demagnetized in an Analytical Service Co. (ASC) thermal demagnetizer and measured in a three-axes cryogenic 2G magnetometer in the field-free room at the University of Michigan's paleomagnetic laboratory. Heating was carried out in 50°C increments to a maximum temperature of 550°C, with reduced increments at temperatures above 350°C. Alternating Field (AF) demagnetization was performed with a Sapphire Instruments SI-4 AF demagnetizer; however, the AF treatment was unable to isolate the principal components of the remanence properly. In the thermally treated samples, remanence directions were calculated from Principal Component Analysis (Kirschvink, 1980) of linear demagnetization vectors picked from paleomagnetic orthogonal projection plots (Zijderveld, 1967). In those cases in which a site had more than two magnetization components, the Hoffman and Day (1978) great-circle method was used to isolate the remanence directions.

Site means were calculated by averaging the sample set directions, using the method of Fisher (1953). Inclination-only (Parés et al., 1994) and local fold tests (McElhinny, 1964) were used to characterize the age of the magnetization components with respect to folding in the individual domains. However, because of the local declination scatter caused by (sub)vertical axis rotations, the inclination-only test was predominantly used. With this test it is possible to account for the statistically significant clustering of inclinations after partial or full tectonic correction, independent of the declination scatter produced by vertical axis rotation (McFadden and Reid, 1982).

4. Results

The Santa Lucia and Portilla limestones have similar demagnetization characteristics and the two formations will be treated together in the following discussion. The results from demagnetization for all three structural domains are presented in Table 1. Two magnetizations are distinguished, in addition to the present-day field overprint: an early Permian (B) component, and a Late Carboniferous (C) component. This age assignment is the same as that used by Van der Voo et al. (1997). The present-day field A magnetization, which is northerly and down, has a low unblocking temperature and is removed by 250°C. This is followed by the intermediate B magnetization, which has a mean inclination of $+1.5^\circ \pm 3.1^\circ$ (as calculated by Van der Voo et al., 1997), and an unblocking temperature up to 480°C. The C magnetization has a mean inclination of $+5.0^\circ \pm 6.6^\circ$ (as calculated by Van der Voo et al., 1997), and unblocks at temperatures up to 50°C.

4.1. Tectonic corrections

Due to the complexity of superimposed-folding in the area, a method was devised to determine the optimal tectonic correction for individual site mean directions. Each sampling site was evaluated in the context of the local structures to determine the best possible correction to undo post-magnetization tilts and rotations. Within individual structural domains, deformation axes were determined by calculating the best-fit rotation axes to cluster in-situ magnetic vectors. This is similar to the approach used by Setiabudidaya et al. (1994) and Stewart (1995) to reconstruct complex fold geometries in comparable structures. The observed girdle distributions represent the differential rotation of F_3 fold limbs in the case of the B component, and the rotations produced by F_2 and F_3 deformation for the C component subsequent to magnetization acquisition. By definition, the distributions of in-situ magnetic vectors produced by folding will track small-circles that contain the original reference magnetic direction (i.e. the mean B or C magnetic direction acquired prior to folding). Coincidentally, in most structures studied it was found that the reference direction was positioned

Table 1
Paleomagnetic and structural site information and statistical parameters

Site	No. Cores	*Tectonic Corrections*				*In Situ Site Mean*							
		Strike	Inv. Dip	Dip Dir.	Dip	Dec (Low-Temp)	Inc (Low-Temp)	alpha 95	K	Dec (High-Temp)	Inc (High-Temp)	alpha 95	K
La Queta Syncline													
PL26	8	318		48	48					142	11	7	108
PL27[a]	8	170	99	80	81					134	−4	6	110
PL28	8	145		235	84					123	−2	4	284
PL29	8	97		187	52					102	43	3	938
PL30[a]	8	170	95	80	85					111	−27	5	170
PL31[a]	8	137	92	47	88					88	−17	10	44
PL32	8	300		30	58					140	−5	3	437
PL33	8	30		120	52					73	53	4	326
PL34	8	335		65	55					88	59	5	177
PL35	8	275		5	35					141	20	6	187
PL36	8	310		40	40					134	−1	6	75
PL37	8	110		200	38					110	38	6	48
PL38	8	191		281	78					143	8	9	48
La Vega de los Viejos Syncline													
SL56[b]	6	(108		198	58)	(88	22)	9	60	(46	3)	9	61
SL57[b]	6	(80		170	85)					(44	−34)	16	19
SL58[d]	7	112		202	62	125	−14	11	27	77	−20	9	67
SL59[b]	7	(166		256	60)					(66	−42)	10	38
SL60[ad]	7	(243	135	153	45)	(321	−52)	14	15	(357	−67)	8	66
SL61	5	135		225	68					80	−41	5	117
SL62	6	143		53	90					103	−34	3	487
SL64[d]	8	114		204	50	110	14	9	42	93	13	7	66
SL65	8	120		210	84					122	13	9	37
SL66	8	164		254	85					126	−15	4	167
SL67	6	344		74	80					143	−2	6	66
SL68	6	352		82	80					117	32	13	54
SL69[d]	9	355		85	77	125	11	6	76	97	20	6	71
SL70	6	355		85	70					119	−4	5	273
SL71	8	354		84	74					140	−5	12	21
PL49	7	238		328	69					117	−47	5	125
PL50	5	120		210	51					82	−32	10	64
PL51[d]	8	145		235	78	132	−24	9	32	93	−27	6	86
PL52[ad]	8	146	94	56	86	145	−39	14	20	114	−42	10	33
PL53	6	105		195	64					106	6	13	34
PL54[a]	8	152	99	62	81					129	−34	6	70
PL55[d]	6	125		215	60	120	2	3	626	102	4	8	80
PL56[d]	5	114		204	41	112	10	5	154	104	14	5	130
PL57	8	21		111	55					108	18	10	40
Proza Anticline													
SL38	8	250		340	54	190	−40	6	114				
SL39[a]	8	142	105	52	75	123	−16	4	281				
SL40[c]	9	20		110	74	202	12	11					
SL41w	4	200		290	70	147	3	11	35				
SL41e	5	360		90	76	129	6	11	29				
SL42[b]	8	358		88	80	(194	−41)	6	128	(180	−63)	8	48
SL43	8	45		135	78	215	24	7	73				
SL44	9	155		245	39	136	12	5	182				
SL45	7	238		328	45	175	−12	7	71				
SL46	8	148		238	47	125	15	8	53				
SL47	8	205		295	47	174	37	8	70				
SL48	8	216		306	67	168	−11	3	704				
SL72[c]	9	218		308	63	186	−22	8					
SL73	6	214		304	62	187	−5	8	80				
SL74	6	221		311	48	177	−8	4	246				
SL75[ab]	7	353	102	263	78	(193	27)	6	75				
SL76	8	45		135	63	225	59	5	294				

(continued on next page)

Table 1 (*continued*)

Site	No. Cores	*Tectonic Corrections*				*In Situ Site Mean*							
		Strike	Inv. Dip	Dip Dir.	Dip	Dec (Low-Temp)	Inc (Low-Temp)	alpha 95	K	Dec (High-Temp)	Inc (High-Temp)	alpha 95	K
SL77[b]	5	14		104	46								
SL78[a]	9	27	115	297	65	215	34	6	67				
SL79[a]	6	50	100	320	80	220	6	5	220				
SL80	8	210		300	74	149	−50	4	32				
SL81	6	332		62	70	154	8	4	244				
SL82	8	113		203	51	106	−10	8	131				

[a] Designates overturned bedding.
[b] Designates a site that could not be used (explained in text).
[c] Designates a site that required great-circle analysis.
[d] Designates a site that required Hoffman Day (1978) analysis. (Dec, Inc) Represents paleomagnetic data not used in analysis (explained in text).

relative to the distributed magnetic vectors, such that the Euler pole of rotation was approximately 90° away. This geometric configuration resulted in the unique case where the best fit small-circle is a great-circle. Note that we assume no significant rotation about the axis of the (south-southeasterly and shallow) magnetization, which cannot be detected by this analysis. However, such a rotation would lead to recumbent folds, which are not observed in our field area or recognized in the literature. Using the calculated F_3 axes, F_3 deformation can be removed and the geometry of the CAA's hinge zone restored to the time of magnetic acquisition. Consequently, this correction process constrains the kinematics of F_3 folding, as well as a reconstruction of the CAA's geometry after F_2 deformation in the case of the B component, and after F_1 deformation in the case of the C component.

4.2. La Queta Syncline

Thirteen sites were collected around the La Queta Domain (Fig. 2). All sites are located in the Portilla Formation, which has continuous exposure around the entire structure. The in situ magnetic directions show a correlation between site mean declination and local strike, and an inclination pattern that ranges from mainly upward in the south to steep and downward in the north (as listed in Table 1). Typical orthogonal projection plots and site means for the La Queta Syncline are shown in Figs. 5(a) and 6. After removal of a viscous present-day field overprint, one stable ancient component was found within the La Queta Domain (Fig. 5a).

The geometry of the La Queta Syncline only permits fold tests on kilometer-scale folds. A total of four fold tests were performed: (1) on the southern tip; (2) on the northeast corner; (3) on a north-wall interference fold; and (4) on the entire central zone of the main synclinal structure. In the southern tip of the La Queta Domain the structure becomes tightened, and the limbs take on a (sub)parallel orientation. However, because of the magnetic declination scatter in the southern tip (sites PL26, PL31 and PL32), it is only possible to perform an inclination test (Fig. 7a). The axis of the fold trends northwest–southeast and is probably related to F_1 and F_2 deformation because of its orientation. At 35% unfolding, the inclinations cluster at +7° with a maximum kappa value of 149 (Fig. 7a). This result is interpreted as a C component that is post-F_1 deformation but pre-F_2 and -F_3 deformation.

Similar fold tests were done on the smaller (sub)parallel folds found in the northern and northeastern regions of the syncline: between sites PL29 and PL33, and sites PL37 and PL38 (Fig. 7b and c). Upon correction (inclination only), sites PL29 and PL33 cluster at 35% unfolding with an inclination of +39° (kappa = 19,130), and sites PL37 and PL38 cluster at 50% unfolding with an inclination of +35° (kappa = 10,747). Such high kappa values are caused by a high degree of clustering combined with a low number of sites. Both tests are statistically significant at the 95% confidence level, and are interpreted as a C magnetization that predates F_2 and F_3 deformation. The final fold test was done on the five middle sites (PL27, PL28, PL30, PL35, and PL36), where the in-situ magnetic declinations and local strikes are subparallel on both limbs, and the inclinations exhibit considerable scatter, ranging from +20 to –27° (Fig. 7d). At 40% unfolding the inclinations clustered at +13° (kappa = 25). The results of the four fold tests show a consistent pattern of magnetization acquisition prior to F_2 and F_3 deformation. Given the definition of the C component as post-F_1 and pre-F_2 and -F_3, we interpret the entire La Queta structure as carrying the C magnetization.

Therefore, the C magnetization is used as a rotation constraint, to find those structural corrections that

bring the in-situ magnetic directions into coincidence with the reference C magnetization. These structural corrections thereby undo the deformation (tilts and rotations) that the rocks have undergone since the acquisition of the C-component remanence (i.e. F_2 and F_3 folding). By iterating the possible fold geometries that would result in both the La Queta's present-day bedding attitudes and its in-situ magnetic direction scatter, an optimum set of fold-axes were calculated to correct for F_2 and F_3 deformation.

Using the best-fit rotation axis (Fig. 6c and d), tilt-corrected site means and post-remanence bedding attitudes were calculated for the northern sites (PL29, PL33, PL34, PL35, PL37, and PL38) and southern sites (PL26, PL27, PL28, PL30, PL31, PL32, and PL36) of the La Queta syncline (Fig. 6b). When applied, these corrections create a broad north–south-oriented syncline with intermediately to steeply dipping limbs, and a slightly northward-plunging fold axis (Fig. 8), thereby restoring the syncline to its post-F_1 geometry (corrected bedding and magnetic direction are listed in Table 2). The applied rotations, corrected declination, inclinations and bedding are given in Table 2.

4.3. La Vega de los Viejos Syncline

Twenty-four sites were collected around the La Vega de los Viejos Domain (Fig. 3). Fifteen sites are located in the Santa Lucia Formation and nine sites are located in the Portilla Formation. Of the 24 sites, the four southernmost sites could not be interpreted (SL56, SL57, SL59 and SL60) due to clearly rotated bedding relative to regional trends caused by complicated local fault rotation (Fig. 3). Both formations have continuous exposure around

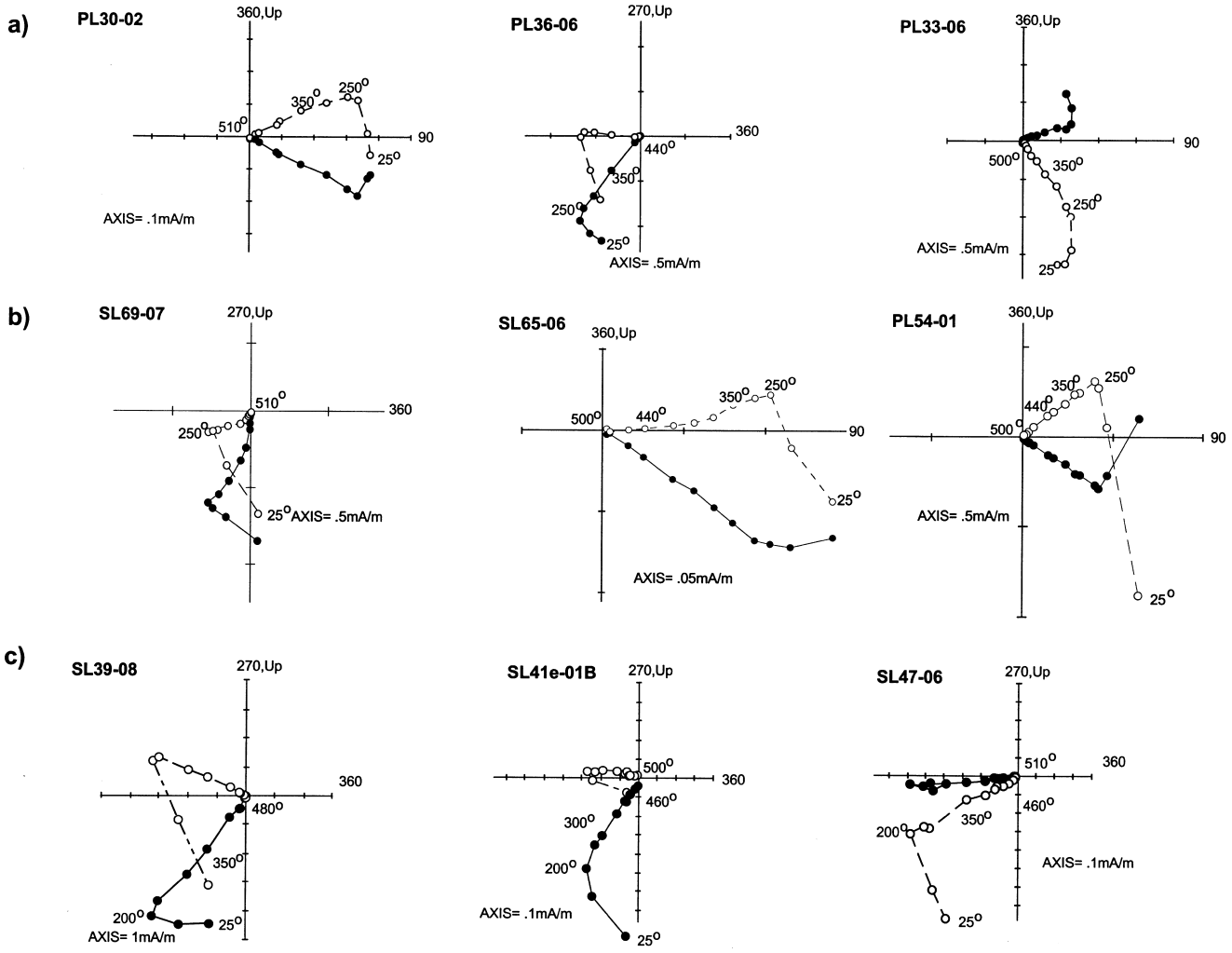

Fig. 5. Typical examples of orthogonal thermal demagnetization plots (Zijderveld, 1967) in in-situ coordinates from nine Devonian limestone samples from the Portilla and Santa Lucia formations. Open (closed) symbols represent projections onto the vertical (horizontal) plane; demagnetization temperatures given in degrees Celsius. (a) La Queta Syncline samples. (b) La Vega de los Viejos Syncline samples. (c) Proza Anticline samples.

the entire structure except for the southwestern corner, which is covered by Stephanian aged sediments and Quaternary alluvium. Typical orthogonal-projection plots and site means for the La Vega de los Viejos Syncline are shown in Figs. 5(b) and 9(a) and in-situ site means are listed in Table 1. Two ancient components were observed in all but one of the sites. However, in only seven of the sites that carried both components could stable directions be sufficiently characterized for paleomagnetic analysis due to stability spectrum overlapping. To separate the NRM of the low temperature component from the high temperature component, we utilized the Hoffman and Day (1978) method of vector subtraction. The site with only one ancient component is assumed to carry the high temperature remanence. The in-situ magnetic directions show a correlation between site mean declination and local strike, and an inclination pattern that ranges from mainly steep and upward in the south to steep and downward in the north, very similar to the La Queta Syncline to the east (Table 1).

The outcrop of the La Vega de los Viejos Syncline only permits fold tests on kilometer-scale folds. A total of three fold tests were performed (Fig. 10): (1) on the high temperature components of the entire structure except for the southern tip, (2) on the high temperature component of sites PL50 and PL49, and (3) on the low temperature components of two northern sites (SL64 and SL69), one on each limb of the syncline.

The first fold test was an inclination-only test done on the high temperature components of sites

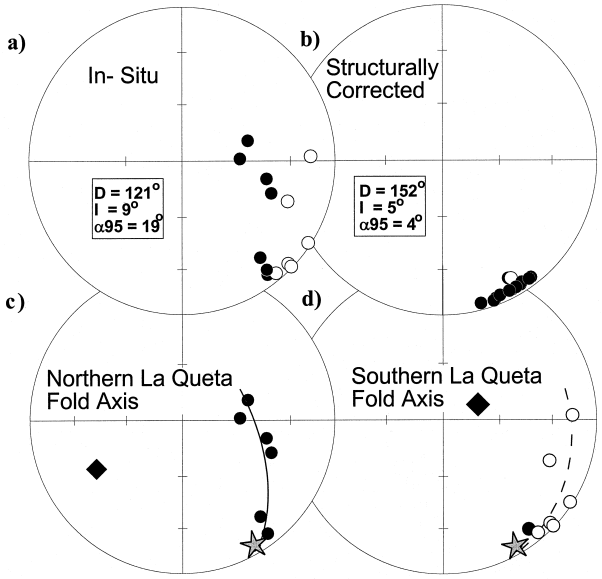

Fig. 6. La Queta site mean stereonet projections for (a) in-situ and (b) structurally corrected magnetic directions. Open symbols represent upper hemisphere projections and closed symbols represent lower hemisphere projections. (c) Calculated fold axis for the northern La Queta structure to correct for F_2 and F_3 folding. Circles are site-means and diamonds represent best-fit fold axes (lower hemisphere). Gray star represents the reference direction for the C component. (d) Calculated fold-axis for the southern La Queta structure used to correct for F_2 and F_3 folding. Notice the change in fold-axis orientation from south to north to accommodate the complex paleomagnetic direction distribution. Gray star represents the reference direction for the C component.

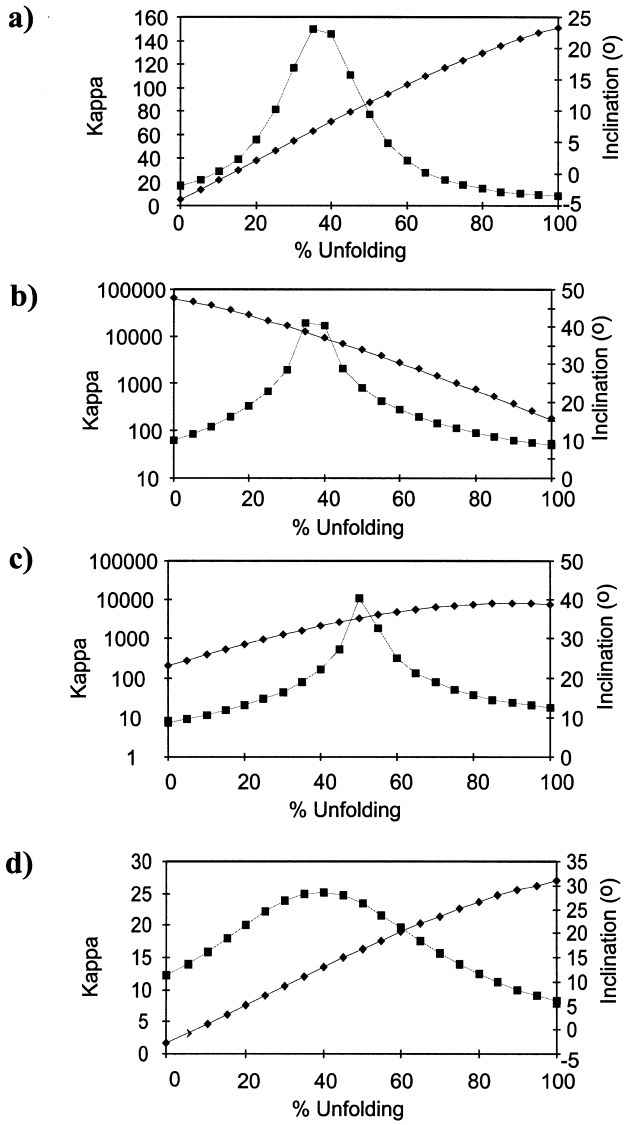

Fig. 7. Local incremental inclination-only fold tests from the La Queta Syncline, plotting the kappa parameter (squares) and inclination (diamonds) vs. percent unfolding. (a) A local fold test of sites PL26, PL31, and PL32 showing a C component acquired pre-F_2 folding, yielding a 6° inclination at 35% unfolding. (b) A local fold test of sites PL29 and PL33 showing a C component acquired syn-folding with high (~39°) inclination values at 35% unfolding. (c) A local fold test of sites PL37 and PL38 showing a C component acquired pre-F_2 with a high inclination value (~35°) at 50% unfolding. (d) A local fold test of middle sites showing a C component acquired pre-F_2 with intermediate positive inclination values (~13°) at 40% unfolding.

PL51, PL52, PL53, PL54, PL55, PL56, PL57, SL61, SL62, SL64, SL65, SL66, SL67, SL68, SL69, SL70, and SL71 (Fig. 10a). The in-situ magnetic declinations range from easterly on the eastern limb to southeasterly on the western limb, with local strike having approximately 40° of curvature on the eastern limb. The inclinations between the 17 sites exhibit considerable scatter, ranging from +32° to –42°. At 40% unfolding the inclinations clustered at –6° (kappa = 18). This result is consistent with a C magnetization acquisition that is pre-F_2 deformation. A second inclination-only fold test was done on the high temperature components of sites PL49 and PL50 (Fig. 10b). These two sites define an east–west-trending fold in the southern most section of the Viejos structure (Fig. 3). At 55% unfolding the inclinations clustered at –13° with a high kappa value, consistent with (C) magnetization acquisition prior to F_2 folding. Both fold tests produce mean inclinations that are slightly different from the expected reference direction, which we attribute to tilting subsequent to magnetization acquisition.

The third inclination-only fold test was done in the northern section of the Viejos domain on two sites that carry the low temperature component: sites SL69 and SL64 (Fig. 10c). At 0% unfolding the inclinations clustered at +13° (kappa = 730). Again, the somewhat higher than expected inclination is attributed to tilting subsequent to magnetization acquisition. The fact that all low temperature site means consistently exhibit less rotation away from the reference direction (Table 1), coupled with the above post-folding fold test result, suggests that the low temperature component found in the Viejos Syncline corresponds to a B magnetization acquired post-F_2 folding. Due to the scarcity of low temperature (B) components, further fold tests could not be performed.

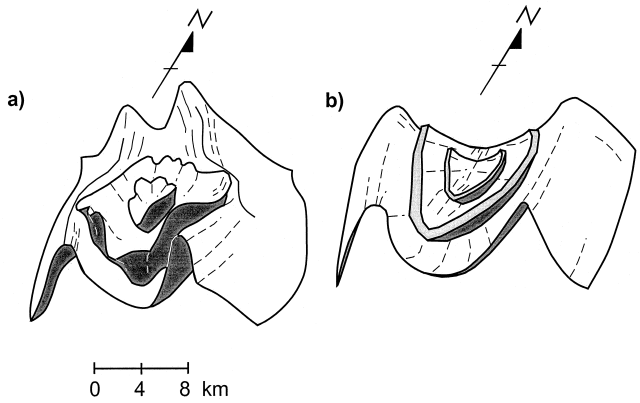

Fig. 8. Schematic 3-D drawing of the La Queta Syncline in its present configuration (after Julivert and Marcos, 1973) (a), and corrected to its post-F_1 configuration according to the calculated fold axes of the north and south La Queta structure (b). Individual bedding was rotated according to the tilts and rotations indicated by the deviating site-mean directions of the magnetizations (see Table 2 for rotation parameters). After correction the La Queta syncline becomes less contorted and takes on a more cylindrical north–south trend.

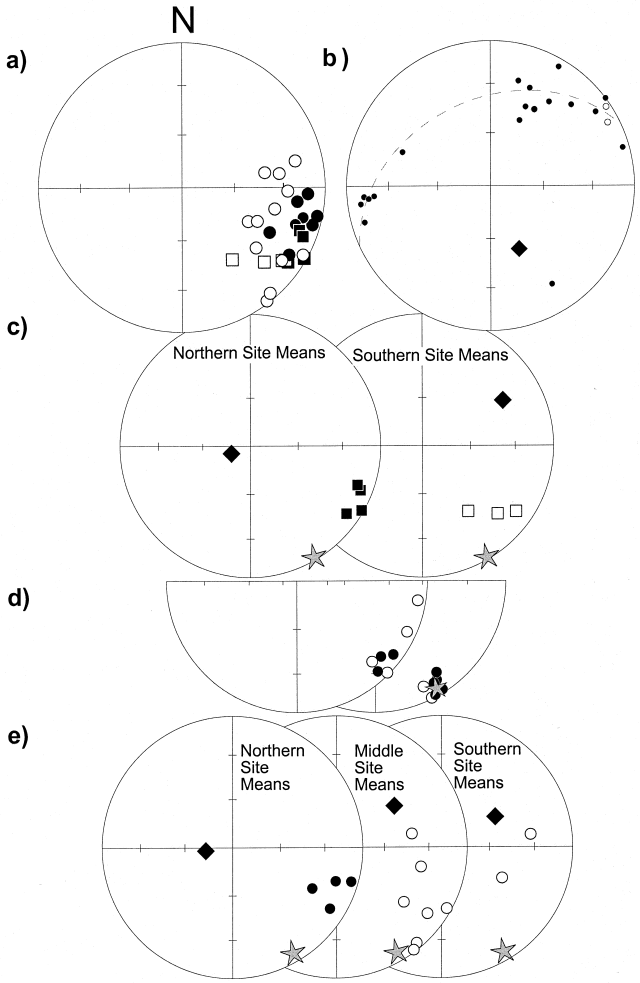

Fig. 9. La Vega de los Viejos site-mean stereonet projections for poles to bedding and in-situ magnetic directions. Open symbols represent upper hemisphere projections and closed symbols represent lower hemisphere projections. (a) Stereonet of in-situ site means for the entire Viejos structural domain. Circles correspond to high-temperature components (C), and squares correspond to low temperature components (B). (b) In-situ poles to bedding for the entire Viejos structure with fold axis shown as black diamond. Overturned beds projected as upper hemisphere poles. (c) B component site-mean directions for the northern and southern sections of the Viejos domain with best-fit rotation axes (represented by black diamonds). Gray stars represent reference B direction. (d) The two-step C component correction for those sites that carry both the B and C magnetizations. The left stereonet shows the C components rotated with the B magnetization leaving F_2 deformation to correct for. The right stereonet shows the fully corrected C components after F_2 folding is corrected for. Rotation parameters are listed in Table 3. (e) Stereographic projections of site means that only carry the stable C component for the northern, middle and southern sections of the Viejos domain with best-fit rotation axes (fold axes represented by black diamonds). Gray stars represent reference C direction.

Table 2
Summary of structurally corrected site information[a]

Site Number	*In Situ Bedding*			*Tectonic Correction*			*Tectonically Corrected*			
	Strike	Inv. Dip	Dip	Fold Axis Trend	Fold Axis Plunge	Rotation	Dec	Inc	Strike	Dip
La Queta Syncline										
PL26	318		48	65	70	10	151	14	330	47
PL27[b]	170	99	81	65	70	27	159	5	196	94
PL28	145		84	65	70	27	148	6	169	84
PL29	97		52	242	36	52	144	6	171	38
PL30[b]	170	95	85	65	70	45	150	−13	213	86
PL31[b]	137	92	88	65	70	75	160	4	217	81
PL32	300		58	65	70	27	165	5	331	55
PL33	30		52	242	36	75	147	7	306	9
PL34	335		55	242	36	75	157	6	335	55
PL35	275		35	242	36	17	150	6	276	46
PL36	310		40	65	70	20	153	6	337	39
PL37	110		38	242	36	44	143	6	187	36
PL38	191		78	242	36	2	144	6	192	79
La Vega de los Viejos Syncline										
SL58	112		62	60	30	32	141	12	120	78
SL58H[c]	112		62	67	63	67	148	3	167	72
SL61H	135		68	55	45	81	150	8	184	74
SL62H	143		90	55	45	61	151	6	183	76
SL64	114		50	249	77	34	144	8	154	47
SL64H[c]	114		50	284	81	51	148	12	169	44
SL65H	120		84	264	73	30	151	6	150	79
SL66H	164		85	55	45	33	150	8	184	74
SL67H	344		80	55	45	12	152	6	354	83
SL68H	352		80	264	73	30	149	25	19	77
SL69	355		77	249	77	34	158	4	27	73
SL69H[c]	355		77	276	81	46	146	17	40	75
SL70H	355		70	55	45	30	140	17	20	84
SL71H	354		74	55	45	15	151	6	7	80
PL49H	238		69	60	51	75	150	7	325	34
PL50H	120		51	60	51	35	150	7	133	60
PL51	145		78	60	30	32	149	3	155	78
PL51H[c]	145		78	66	59	65	154	0	193	70
PL52[b]	146	94	86	60	30	32	161	−11	164	93
PL52H[bc]	146	94	86	63	49	46	155	−13	183	89
PL53H	105		64	264	73	45	150	−3	154	55
PL54H[b]	152	99	81	55	45	34	154	−10	178	90
PL55	125		60	249	77	34	153	−5	164	58
PL55H[c]	125		60	284	81	51	152	2	180	55
PL56	114		41	249	77	34	145	3	157	38
PL56H[c]	114		41	274	81	45	150	11	167	36
PL57H	21		55	264	73	40	144	10	53	47
Proza Anticline										
SL38	250		54	236	49	−50	146	−10	205	22
SL39[b]	142	105	75	45	50	33	149	6	171	96
SL40[d]	20		74	62	34	−26	159	−8	330	71
SL41w	200		70	236	49	−4	150	0	196	68
SL41e	360		76	236	49	29	149	−10	17	63
SL43[e]	45		78	60	45	−24	148	6	334	74
SL44	155		39	236	49	18	150	1	181	43
SL45	238		45	236	49	−28	153	5	212	27
SL46	148		47	236	49	32	150	−5	188	55
SL47	205		47	45	50	−33	145	18	186	65
SL48[d]	216		67	62	34	16	149	2	191	65
SL72[e]	218		63	60	45	32	159	1	183	42
SL73[e]	214		62	60	45	9	143	2	170	58
SL74[d]	221		48	62	34	11	155	2	192	42
SL76[d]	45		63	62	34	−48	148	7	323	50

Table 2 (*continued*)

Site Number	*In Situ Bedding*			*Tectonic Correction*			*Tectonically Corrected*			
	Strike	Inv. Dip	Dip	Fold Axis Trend	Fold Axis Plunge	Rotation	Dec	Inc	Strike	Dip
SL78[bd]	27	115	65	62	34	−43	148	2	346	101
SL79[be]	50	100	80	60	45	32	155	−8	347	94
SL80	210		74	210	0	56	139	5	210	15
SL81	332		70	332	0	60	146	5	332	14
SL82	113		51	45	50	51	146	22	130	59

[a] H — High temperature component.
[b] Designates overturned bedding.
[c] First rotated with B magnetization as stated in text and shown in Table 3.
[d] First rotated about a vertical axis −28°.
[e] First rotated about a vertical axis −50°.

From the above results we use the previously determined B magnetization direction (Van der Voo et al., 1997) as a reference for the in-situ low temperature components, and the C magnetization direction as a reference for the in-situ high temperature components. By iterating the different possible fold geometries that would result in both the La Vega de los Viejos's present-day bedding attitudes (Fig. 9b) and its in-situ magnetic direction scatter (Fig. 9a), an optimum set of fold-axes can be determined (Fig. 9c and e).

Two fold-axes were calculated to bring all low temperature (B) magnetic vectors into coincidence: a northern axis that accommodates sites SL64, SL69, PL55, and PL56, and a southern axis that accommodates sites SL58, PL51, and PL52 (Fig. 9c). Both rotation axes have an approximately east–west orientation and the amount of total rotation required is, on average, approximately 25° less than that needed for the older C component. After correction, the paleomagnetic site means cluster around the reference B direction (Fig. 11a) and the bedding takes on a north–south trend.

To correct for the C component we first analyzed the seven sites that carried stable B and C magnetizations. This allowed the subtraction of rotations that occurred subsequent to the younger B magnetization (i.e. F_3 folding). The additional correction needed to bring the C component into agreement with the reference C direction corresponds to F_2 folding (Fig. 9d). This additional rotation has a component of vertical-axis rotation as seen in the declination scatter, and tilt as seen in the average negative inclination. This secondary correction also defines the difference in kinematics between F_1 and F_2 folding. F_1 folding was strictly about near horizontal north–south-trending fold axes, whereas F_2 was about much steeper axes that produced further tightening of F_1 longitudinal structures, while at the same time adding a small component of vertical-axis rotation. Re-examination of the B and C magnetizations of the Lagos del Valle Syncline to the east (Van der Voo et al., 1997) shows the same kinematic distinction, which suggests that the difference in rotation is not an artifact of limited data but a true contrast in folding kinematics between F_1 and F_2 folding. As an internal check, the two-step rotation method was compared to a one-step rotation for correcting the in-situ C components directly back to the reference C direction (Table 3). The axes of rotation for both correction methods had similar orientations and rotation angles, suggesting that there was little bias between techniques. The remainder of the C component sites that lack adequately determined B components were, of necessity, corrected using only a single composite rotation.

Two fold axes were determined for the remaining sites that carried only the C component magnetic vectors: sites (SL65, SL68, PL53, PL57) from the north, sites (SL61, SL62, SL66, SL67, SL70, SL71, PL54) from the middle and sites (PL49 and PL50) from the south (Fig. 9e). Figs. 9(a) and 11(b) show in-situ and tilt-corrected C component site means, respectively. After applying the same rotations to the in-situ bedding, the La Vega de los Viejos Syncline is restored to its pre-F_2 geometry (bedding and magnetic direction corrections can be found in Table 2). This correction results in a linear north–south-trending syncline (Fig. 11c) similar to the restored La Queta (Fig. 8) and Lagos del Valle Synclines to the northeast (Van der Voo et al., 1997).

4.4. Proza anticline

Twenty-three sites were collected around the Proza Anticline from the Santa Lucia Formation. Ten sites were collected from the east limb, and 13 sites from the western limb (Fig. 4). Typical orthogonal demagnetization plots and site means for the Proza Anticline are shown in Figs. 5(c) and 12. The geologic map pattern of the western limb and partially exposed eastern limb are both characterized by an S-shaped outcrop

pattern. Both limbs also exhibit a consistent relationship between changes in strike and magnetic declination (Fig. 4). However, the inclinations are varied, and change from negative to positive and back to negative along the length of the entire structure (Fig. 13 and Table 1). Such an undulating inclination pattern suggests a combination of southerly and northerly tilts throughout the structure as a result of post-magnetization folding. This pattern is most easily related to a set of variably plunging east–west-trending F_3 fold-axes

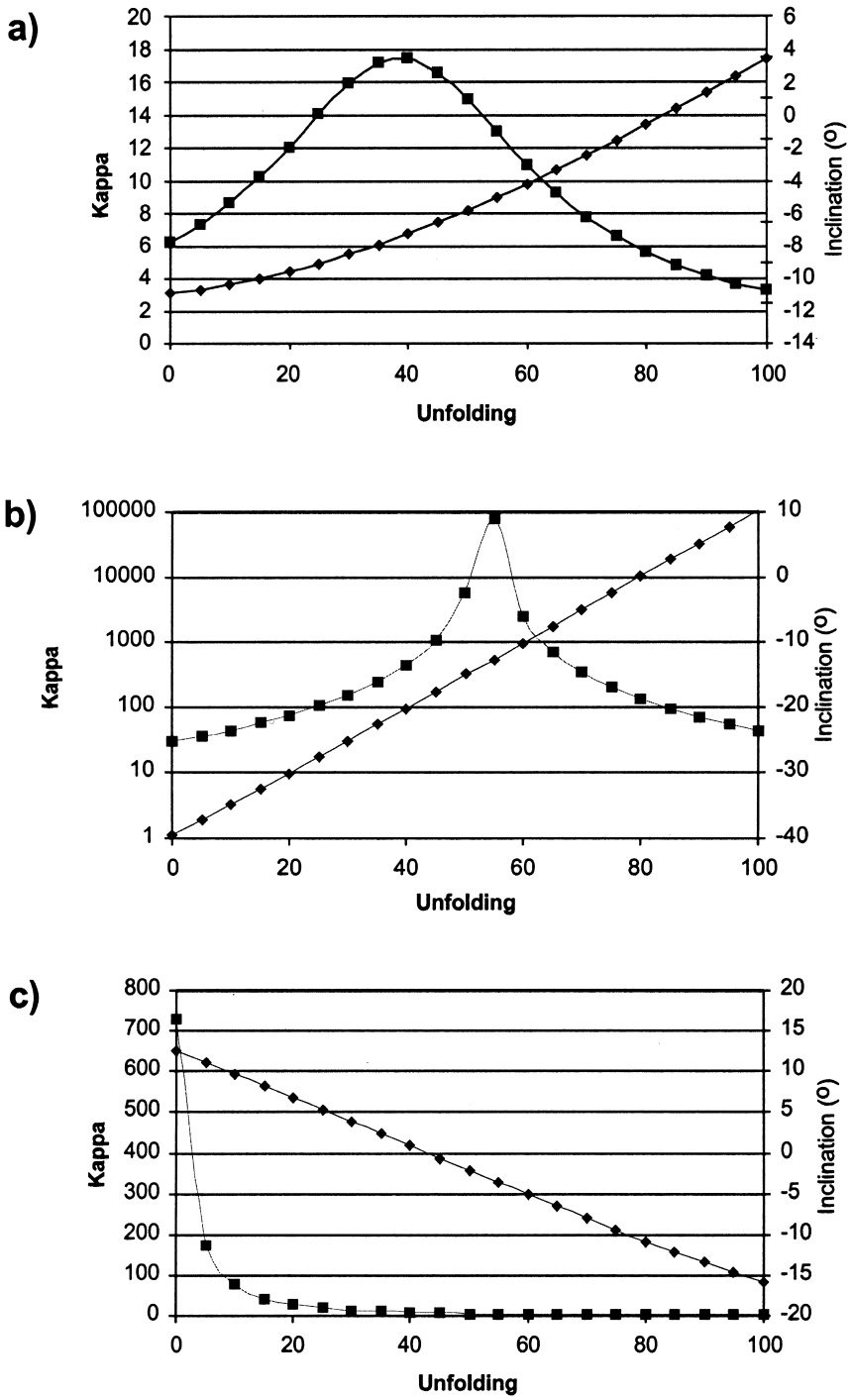

Fig. 10. Local inclination-only fold tests for La Vega de los Viejos Syncline, plotting kappa (squares) and inclination (diamonds) against percent unfolding. (a) Fold test of sites PL51, PL52, PL53, PL54, PL55, PL56, PL57, SL61, SL62, SL64, SL65, SL66, SL67, SL68, SL69, SL70, and SL71 showing a C magnetization acquired pre-F_2 folding. (b) Fold test of sites PL49 and PL50 that also shows a pre-F_2 C magnetization. (c) Fold test for the low temperature component at two sites (SL64 and SL69) in the northern section of the Viejos domain. The maximum kappa at 0% unfolding is consistent with a B component magnetization acquisition that postdates F_2 deformation.

superimposed on an original linear anticline, and is most noticeable in the southern section of the Proza's western limb, where an east–west-trending F_3 fold created an amphitheater structure (Fig. 4). This resulted in a distinct inclination pattern that progressively changes from $+15^\circ$ in the north, to -40° in the south (Fig. 13 between 47 and 57 km).

Three fold tests were performed on the southern sites of the Proza domain. A first fold test was performed on a meter-scale (~10 m) tight anticline in the southern section of the western limb between sites SL41w and SL41e. The anticline has (sub)parallel limbs and a north–south-trending fold axis with an interlimb angle of ~34°, which conforms to early (F_1) folding. The in-situ magnetic directions are southeasterly with shallow inclinations, and upon full tilt correction become more southerly in direction, with steep positive inclinations in the west and negative inclinations in the east. A McElhinny (1964) incremental fold test yielded a maximum kappa at 0% unfolding with a $+5^\circ$ inclination (Fig. 14a), which is interpreted as a B magnetization acquired after F_1 and F_2 folding.

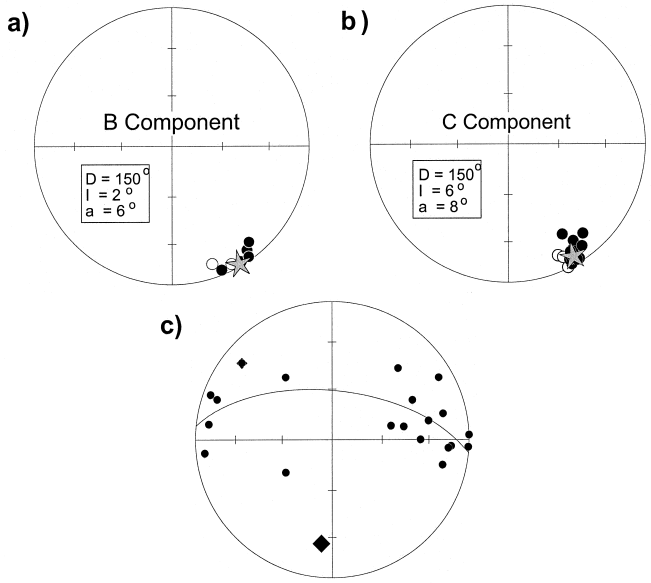

Fig. 11. (a) Stereographic projection of structurally corrected Viejos B component site means using calculated fold axes as stated in text and shown in Fig. 9. Open symbols represent upper hemisphere projections, closed symbols represent lower hemisphere projections and gray stars represent the reference B direction. (b) Structurally corrected Viejos C component site means using calculated fold axes as stated in text and shown in Fig. 9. Open symbols represent upper hemisphere projections, closed symbols represent lower hemisphere projections and white star represents the reference C direction. (c) Poles to corrected bedding (closed symbols) using individually calculated rotation parameters for the C component magnetization (for rotation parameters see Table 2). Also shown is the resultant north–south-trending F_1 fold-axis remaining after the removal of F_2 and F_3 deformation (black diamond).

Table 3
Comparison of rotation axes for Viejos Syncline B and C magnetizations

Site Number	Single Tectonic Correction for C Magnetization			F_3 Tectonic Correction from B magnetization			F_2 Tectonic Correction			Combined Single Tectonic Correction		
	Fold Axis Trend	Fold Axis Plunge	Rotation	Fold Axis Trend	Fold Axis Plunge	Rotation	Fold Axis Trend	Fold Axis Plunge	Rotation	Fold Axis Trend	Fold Axis Plunge	Rotation
SL58	60	51	85	60	30	32	19	78	50	67	63	74
SL64	264	73	57	249	77	34	19	78	17	284	81	51
SL69	264	73	50	249	77	34	19	78	13	276	81	46
PL51	55	45	73	60	30	32	19	78	40	66	59	65
PL52	55	45	67	60	30	32	19	78	19	63	49	46
PL55	264	73	51	249	77	34	19	78	17	284	81	51
PL56	264	73	46	249	77	34	19	78	12	274	81	45

A regional fold test was done on the southern section of the Proza domain between sites SL38, SL39, SL44, SL45, SL46, and SL82 (Fig. 14b). The bedding strikes and magnetic declinations in this region have 95° and 65° of variation, respectively; consequently, a McElhinny (1964) fold test was not used. An inclination-only fold test yielded a maximum clustering at 100% unfolding with a +18° mean inclination (kappa = 26). Given that the fold test was performed on a single limb of an original pre-F_3 anticline, what was actually being tested is whether F_3 folding produced the southern Proza's undulatory inclinations and observed curvature. Thus, the pre-folding result for the single limb is consistent with a B magnetization component that was acquired after F_1 and F_2 folding, but prior to F_3 folding. The final fold test was done on sites SL80 and SL81, which are positioned in a fault-propagation fold at the terminus of the Proza's eastern limb. If, as determined above, the curvature of the southern portion of the Proza is related to F_3 deformation, then it follows that the large thrust that separates the western limb from the eastern limb is associated with space accommodation during F_3 folding. A McElhinny (1964) fold test was performed between the sites resulting in a maximum kappa of 194 at 80% unfolding with a mean inclination of 6° (Fig. 14c). Similar to the previous fold test, this fold test was performed on a single limb of a larger anticlinal structure. Thus, the pre-folding result of the fold test reinforces the conclusion that thrusting of the western limb is contemporaneous with F_3 folding.

Two F_3 fold axes were calculated for the southern and middle portion of the Proza Anticline (for sites SL38, SL41e, SL41w, SL44, SL45, and SL46, and for sites SL39, SL47, and SL82) (Fig. 12b) as dictated by the undulating nature of the observed inclination trend (Fig. 13). No sites were taken from the eastern limb because of the large thrust fault that separates the two limbs east and southeast of site SL47 (see Fig. 4). Using the calculated axes, site means and bedding

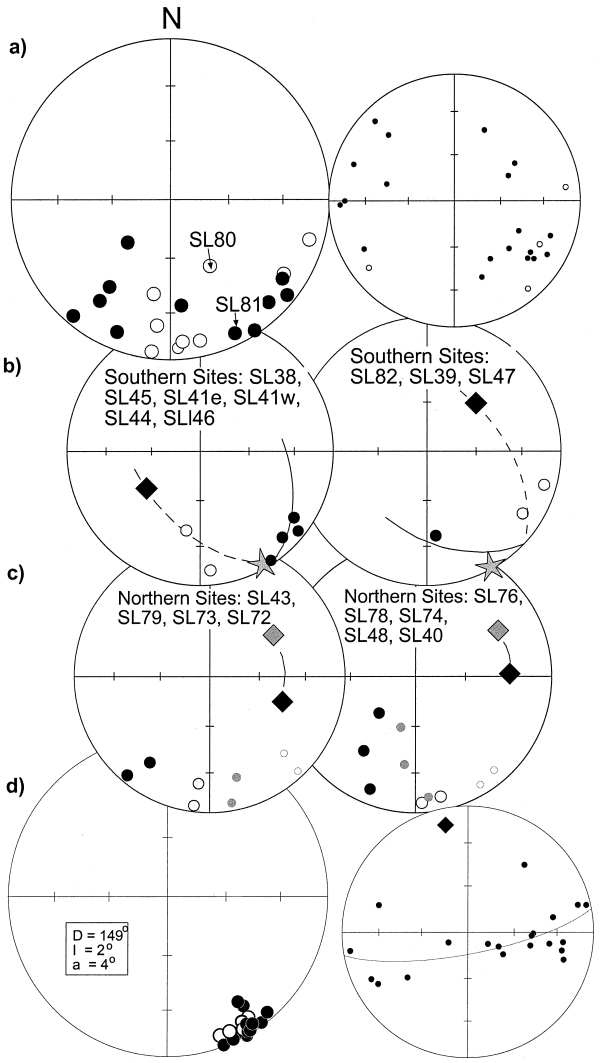

Fig. 12. Stereographic projection of Proza Anticline site means (large circles) and bedding poles (small circles), both in situ and structurally corrected. Open symbols represent upper hemisphere projections and closed symbols represent lower hemisphere projections. (a) Stereographic projection of in-situ northern and southern site means for the Proza structural domain (large net), and stereonet of poles to in-situ bedding for the entire structure (small net). (b) Southern site means with best-fit small-circle (dashed in upper hemisphere and solid in lower hemisphere) and resultant F_3 fold axis (black diamond). (c) Northern site means showing in-situ site means in large circles and vertical-axis rotated site means as small circles (as described in text), and resultant F_3 fold axis (unrotated F_3 fold axes represented by a black diamond). (d) Structurally corrected Proza site means using calculated F_3 fold axes (large net), and corrected poles to bedding (small net). Notice the nearly north–south trend and shallow plunge of the restored pre-F_3 Proza anticline (fold-axis shown as black diamond).

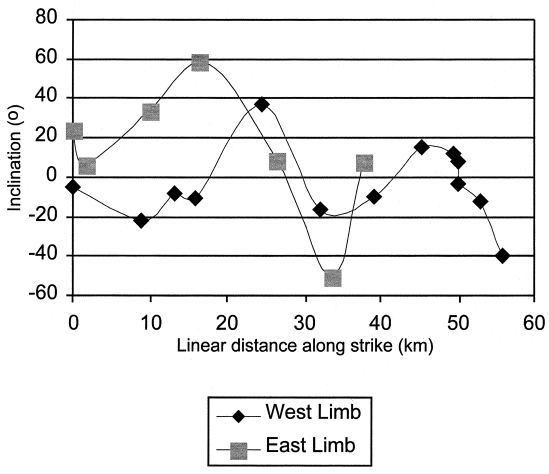

Fig. 13. Plot of inclination vs. linearized distance, from north (0 km) to south (60 km), along structural strike for the east and west limbs of the Proza Anticline. Notice the undulatory pattern imposed by F_3 folding, as well as the repeated pattern of the east and west limb transects. Sites SL77, SL75, and SL42 are excluded as discussed in text.

were corrected as previously explained (Fig. 12d) (see Table 2 for corrected site means and rotation parameters). After correction, the southern half of the Proza anticline transforms from an amphitheater geometry to an almost linear north–south-trending west-dipping fold, similar to the proposed reconstruction of the Lagos del Valle Syncline to the west (Van der Voo et al., 1997).

A similar approach was used for the northern site means on both the west and east limbs of the Proza structure. Two families of site means were distinguished by inclination patterns, sites SL43, SL72, SL73 and SL79 to the north, and sites SL40, SL48, SL74, SL76 and SL78 immediately to the south (Fig. 12c). Three sites in the northern area were not used for structural analysis for the following reasons: (1) SL77 did not provide a stable direction, (2) SL75 was sampled in Carboniferous limestones, and (3) SL42 gave an anomalous direction. All of the northern sites of the Proza domain have experienced clockwise vertical axis rotation, which can be seen in the south to southwesterly directions of the site means and the northeasterly trend of in-situ bedding, but they also underwent tilting, which can be seen in the inclination pattern (Fig. 13, Table 1). In order to correct properly for F_3 deformation, a small-circle was calculated for

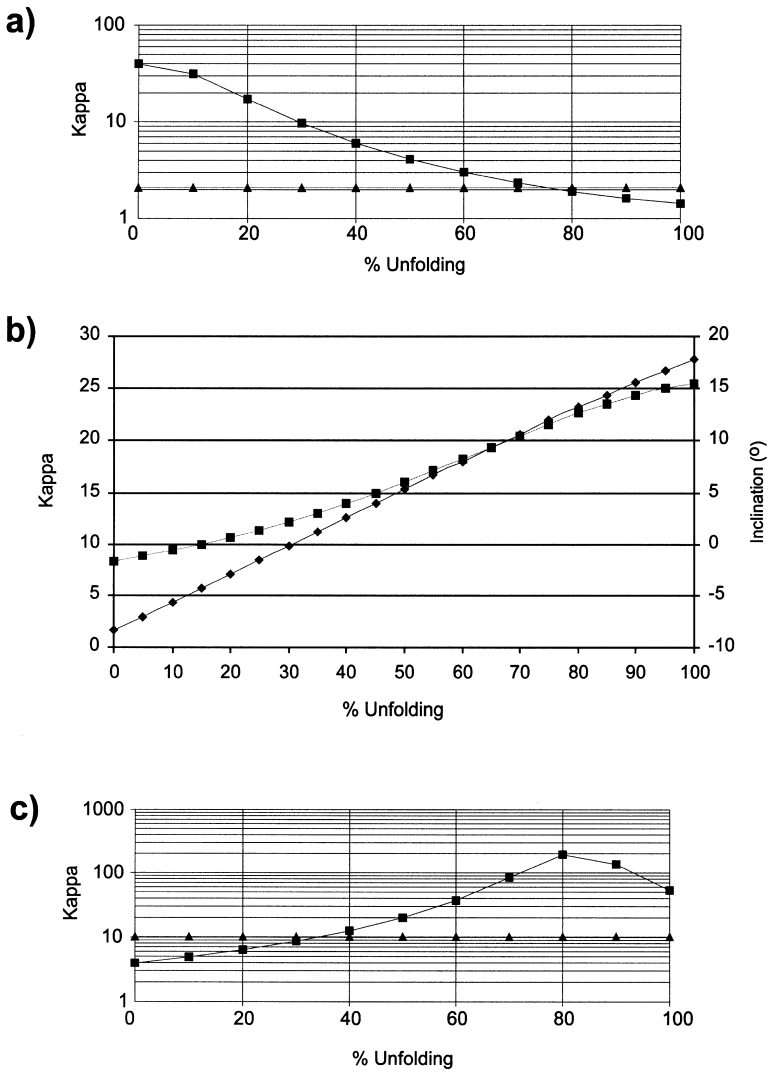

Fig. 14. Local incremental and inclination-only fold tests for the Proza Anticline. (a) A local incremental fold test of sites SL41e and SL41w plotting kappa (squares) and CR (triangles) vs. percent unfolding. The CR parameter is the critical ratio above which the kappa values become significant at the 95% confidence level. The maximum kappa value of 40 at 0% unfolding shows a B component acquired post-folding to F_1 and F_2. (b) An inclination-only test of the southern Proza's western limb, plotting kappa (squares) and inclination (diamonds) vs. percent unfolding. The test yields a maximum kappa value at 100% unfolding. Because all site locations are located on the western limb, this result suggests that F_3 deformation post-dates magnetization acquisition. (c) Incremental fold test between sites SL80 and SL81 in the southern terminus of the Proza's eastern limb. The maximum kappa value is reached at 80% unfolding, consistent with the interpretation that this fold is an F_3 structure related to thrusting of the Proza's western limb over the Proza's eastern limb.

each group, which was then rotated about a vertical axis until the small-circle contained the reference B direction. The Euler pole was then used to correct the magnetizations back to their reference orientation. After correcting all of the Proza in-situ bedding to their pre-F_3 configuration, a linear north–south anticline was restored (compare Fig. 12a and d).

5. Discussion

The magnetization history of the CAA as described above allows discrimination between regional fold generations and determination of the timing and regional kinematics of the main phases of Variscan deformation that affected our study area in northern Spain (Fig. 15).

5.1. Temporal and spatial constraints

Utilizing local and regional fold tests within structural domains, age determinations can be made for folding events by comparing directions of characteristic magnetizations to the late Paleozoic magnetic directions for the stable interiors of Iberia and Europe (Van der Voo, 1993). The first generation of Variscan deformation, F_1, is bracketed by the acquisition of the C magnetization that is Westphalian in age and coincides with a change in sedimentation from shallow marine to clastic (molasse-type) deposits associated with initial orogenic uplift. The second generation, F_2, is bracketed by the age of the C magnetization and the age of the B magnetization, and represents an unconformity and hiatus at the Westphalian–Stephanian boundary (Fig. 15). The associated clastic deposits of Stephanian age form wedges that are predominately made up of carbonate conglomerates, coal measures, and thin red-bed layers that unconformably overlie older stratigraphic units (Julivert, 1971; Pérez-Estaún et al., 1990; Martinez-Garcia, 1991). The deformation of the shallow marine and clastic units constrains the relative ages of the first movements of different thrust sheets, with a lower Westphalian age for the westernmost thrusts and an early Stephanian age for the easternmost thrusts (Pérez-Estaún et al., 1988). The F_3 deformation phase is separated from earlier deformation by the acquisition of the B magnetization, and resulted in a radial fold set and tightening of the arc during Sakmarian to Kungurian (Lower Permian) times. The F_3 phase ended before the Late Permian, as indicated by Permo-Triassic cover rocks that show no major rotation since their deposition (Parés et al., 1996). Thus, the B and C magnetization components found in the hinge zone of the CAA are constrained by local and regional fold-tests as post-F_2 folding and post-F_1 folding, respectively. This differs from the interpretation of Parés et al. (1994), Stewart (1995), and Van der Voo et al. (1997), who did not distinguish between F_1 and F_2 folding and combined them into one generation, and interpreted the acquisition of the C magnetization as synfolding during this single folding event.

The geographical distribution of magnetization components between structural domains suggests regional tectonic control on remagnetization. The B magnetization is present throughout the hinge area in both the outer Somiedo-Correcilla thrust unit and inner La Sobia thrust unit, except for the La Queta domain, whereas the C magnetization seems to be restricted to the outer Somiedo-Correcilla thrust unit only. This pattern, to a first approximation, correlates with the paleotemperature maps of Raven and van der Pluijm (1986) and Bastida et al. (1999) based on the conodont alteration index, suggesting that orogenic fluids may have been responsible for the CAA's variable remagnetization history. Because there is no significant internal strain observed in Devonian limestones of the CAA, rock–fluid interaction during orogenesis was also proposed as the remagnetizing mechanism by Van der Voo et al. (1997). It has been well documented that Paleozoic limestones throughout the Variscan and Alleghanian orogenic belts and foreland basins have experienced widespread remagnetizations (e.g. McCabe and Elmore, 1989; Thominski et al., 1993; Molina-Garza and Zijderveld, 1996).

5.2. Nature of deformation phases in the CAA

Previous studies in the CAA documented an early deformation event that generated both thrusts and longitudinal folds, followed by a second event that

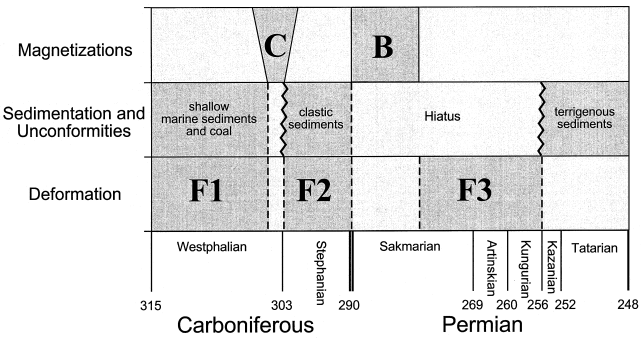

Fig. 15. The Variscan deformation history experienced by the CAA as represented by the three folding phases (F_1, F_2 and F_3), sedimentation record, and the two recorded ancient remagnetizations (B and C components). Age in millions of years is plotted on the horizontal axes for the late Carboniferous and Permian. Deformation phases are bracketed by the age of magnetization and sedimentation as stated in text. Sedimentation record is bracketed by unconformities (zigzag lines) and hiatuses (lighter gray). The times of acquisition of the two magnetizations found in the CAA (darker gray blocks) are known by the comparison of observed mean inclinations with those published for stable Europe.

tightened the region into the arcuate structure we observe today (e.g. Julivert and Marcos, 1973; Julivert and Arboleya, 1984, 1986). Pérez-Estaún et al. (1988) argued that the earlier propagation of thrusts and folds was from west to east, away from the hinterland, as typically observed in fold-and-thrust belts. However, they suggested that the final distribution of thrusting had the spatial properties of a photographic iris, each thrust stacked (and carried inward) in an arcuate arrangement atop the next. Similarly, Julivert and Arboleya (1984) argued for a mechanism in which the individual thrusts had positioned themselves, by a rotational motion, towards the center of the arc during early deformation (F_1 and F_2 in this paper). Importantly, both of these models involve considerable curvature of the CAA prior to F_3 folding. Others have argued that the CAA originated as a linear belt, that later experienced substantial counterclockwise rotation of a single limb during late folding (Ries and Shackleton, 1976; Ries et al., 1980; Bonhommet et al., 1981).

Our work based on paleomagnetism shows that F_3 deformation resulted in arc tightening, refolding, reactivation of major north–south-trending thrusts, and folding of syntectonic Stephanian sediments. Moreover, the need for additional vertical-axis rotation to correct for the C magnetization relative to the B magnetization in those structures carrying both magnetizations, mandates a distinction within the previously defined early deformation phase into two fold generations: F_1 and F_2. This sequence for the initial deformation phase has not been documented in previous studies. In our model F_3 remains geometrically a 'radial' fold set (Julivert and Marcos, 1973), but it is characterized by variably plunging fold-axes, from (sub)horizontal to (sub)vertical, that are imposed on a pre-existing (F_1 and F_2) structural fabric. Thus, F_1 and F_2 structures control the orientation of subsequent F_3 fold axes, which restricts F_3 axes to distinct orientations within a given structural domain. Specifically, F_3 fold axes will vary in orientation based on their location in early folds (F_1 and F_2), but collectively define an axial surface that reflects the regional shortening direction. This contrasts with Stewart (1995), who postulated that the kinematics of F_3 folding was only controlled by the westward-dipping sedimentary layers within the initial thrust stacks and ignored the large-scale folding superimposed on these thrust sheets.

We conclude that the present-day curved geometry of the CAA's hinge zone is established by the interference of original north–south-trending structures,

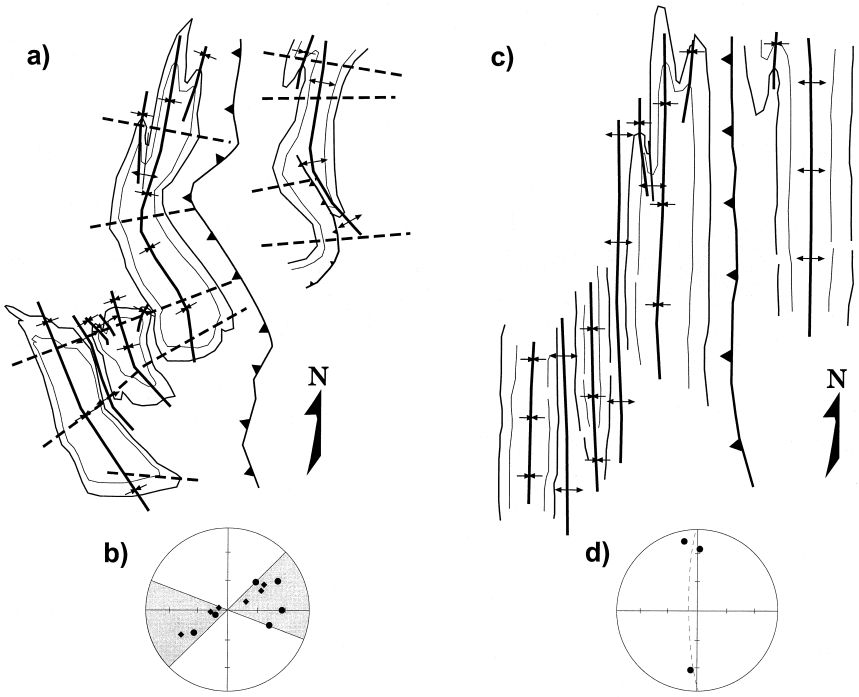

Fig. 16. (a) Schematic structure map of the four structural domains studied in their present-day configuration, including Van der Voo et al.'s (1997) Lagos del Valle Syncline. Highlighted are the refolded F_1 and F_2 axial traces (heavy lines) and F_3 fold axes (dashed lines) calculated in this study. Notice that the F_3 axes are near orthogonal in all cases. (b) Stereonet projection of correction fold axes, as described in text and as listed in Table 2. Black diamonds represent those axes that correct for both F_2 and F_3 deformation, and closed circles represent those axes that correct for only F_3 deformation. (c) Schematic map of pre-F_3 CAA configuration based on bedding orientation calculations from this study. (d) Stereonet projection of pre-F_3 fold axes restored after correction for F_3 deformation. Notice the shallow north–south trend of axes and resultant steep axial surface.

with superimposed F_3 folding about variably plunging east–west axes (Figs. 8 and 16). Regionally, this superposition is caused by a change in the overall shortening direction from east–west in the Carboniferous to north–south in the Permian (in present-day coordinates). In the La Queta, La Vega de los Viejos and Lagos de Valle (Van der Voo et al., 1997) synclines, F_3 fold axes change from intermediately plunging in the north to (sub)vertical in the south. In these three structures, F_3 fold axes all lie approximately in east–west axial surfaces (Fig. 16b). The en échelon arrangement of the three synclines (Figs. 1 and 16a), and the similarity of their F_3 geometry, suggests that F_3 folding systematically affected entire thrust units within the CAA. Originally broad synclines and tight anticlines that formed by F_1 and F_2 folding were transformed into large sinuous basins and tightly buckled anticlines during F_3 folding (Fig. 16a and c). This type of configuration, which is seen throughout the fold-and-thrust province of the CAA, requires originally open cylindrical folds with variable wavelengths and amplitudes (Ramsay, 1960, 1962; Julivert and Marcos, 1973). Such a geometry allows later F_3 folding to refold the limbs of these early structures (F_1+F_2) around variably plunging axes (i.e. the La Queta Syncline), causing oroclinal bending with an overall clockwise rotation in the north and a counterclockwise rotation in the south.

Our work further shows that fault reactivation during F_3 folding caused thrust-sheets to rotate and F_1 and F_2 folds to buckle. As a consequence, there is increased thrust stacking and shortening during F_3, which produced steepened bedding, thrust propagation and arc tightening (oroclinal bending). The Proza Anticline of the inner Sobia thrust unit is a good example of an early F_1+F_2 structure that has been breached, thrust and tightened during F_3 deformation (Fig. 1). Both structural trend and magnetic declination have experienced up to 90° of relative rotation during F_3 folding. According to the paleomagnetic analysis presented here, an originally linear north–south anticline was formed during F_1+F_2 deformation, which was later folded by F_3 deformation. This oroclinal style of rotation resulted in a radial set of east–west-trending F_3 folds, and, due to space problems in the hinge area, thrust initiation and propagation in the southern half of the structure. Thus, the curvature observed today in this structure is primarily due to the interference of fold generations (F_1+F_2 and F_3), and not a primary feature created during thrust emplacement, as suggested by Julivert and Marcos (1973), Julivert and Arboleya (1984) and Pérez-Estaún et al. (1988). Their scenarios leave the CAA's hinge zone with significant curvature prior to F_3 deformation, whereas the paleomagnetic data suggest that the hinge zone of the CAA was essentially linear after F_1+F_2 folding and thrusting.

6. Conclusions

We find that on the regional scale, the kinematics of the Cantabria–Asturias Arc is more complicated than indicated by earlier paleomagnetic studies (Bonhommet et al., 1981; Perroud, 1982, 1986; Hirt et al., 1992; Parés et al., 1994; Stewart, 1995). The suggestion of late tightening (F_3) about vertical axes is too simplistic to account for the observed local structural perturbations, which include rotations, tilts, and combinations of the two. Our observations are also not consistent with the idea that the CAA's curvature is the result of continuous rotation of individual thrust sheets about pivotal rotation axes during initial thrusting (Pérez-Estaún et al., 1988). The early phase of deformation can be characterized by two folding generations (F_1 and F_2) based on remagnetization events. During F_3 folding the early F_1 and F_2 structural fabric caused F_3 fold axes to take on variable orientations that resulted in complex geometries within and between individual structural domains.

The mechanism for producing the curvature we see today in the CAA (oroclinal bending) was largely an early Permian north–south shortening event (F_3), which produced both vertical-axis rotations and tilts of original F_1 and F_2 structures in the hinge zone of the CAA. This multiphase deformation history ultimately resulted in tightening of the belt from its pre-F_2 linear configuration (Fig. 16). On a broader scale, the change in regional shortening direction from east–west during F_1 to north–south during F_3 suggests that late deformation required regional compression (or transpression) of Iberia between a northern Laurasian block and a southern Gondwana block. The origin of this change in tectonic regime may reflect late transpressional activity during final Pangea amalgamation, possibly related to a proposed continent-scale mega-shear in the North Atlantic region (Arthaud and Matte, 1977; Ponce de Leon and Choukroune, 1980; Burg et al., 1981; Matte, 1986).

Acknowledgements

This work was supported by the National Science Foundation, Division of Earth Sciences, grants EAR 9705755 and 9508316. The Scott Turner Fund, Department of Geological Sciences, University of Michigan provided summer field support in 1996 and 1997. We thank B. Luyendyk and A. Pérez-Estaún for their reviews.

References

Aller, J., Gallastegui, J., 1995. Analysis of kilometric scale superposed folding in the Central Coal Basin (Cantabrian Zone, NW Spain). Journal of Structural Geology 17, 961–969.

Alvarez-Marrón, J., 1995. Three-dimensional geometry and interference of fault-bend folds: Examples from the Ponga Unit, Variscan Belt, NW Spain. Journal of Structural Geology 17, 549–560.

Arthaud, F., Matte, P., 1977. Late Paleozoic strike-slip faulting in southern Europe and northern Africa: Results of a right-lateral shear zone between the Appalachians and the Urals. Geological Society of America Bulletin 88, 1305–1320.

Bachtadse, V., Van der Voo, R., 1986. Paleomagnetic evidence for crustal and thin-skinned rotations in the European Hercynides. Geophysical Research Letters 13, 161–164.

Bastida, F., Brime, C., García-López, S., Sarmiento, G.N., 1999. Tectono-thermal evolution in a region with thin-skinned tectonics: the western nappes in the Cantabrian Zone (Variscan belt of NW Spain). International Journal of Earth Sciences 88, 34–48.

Bonhommet, N., Cobbold, P.R., Perroud, H., Richardson, A., 1981. Paleomagnetism and cross-folding in a key area of the Asturian Arc (Spain). Journal of Geophysical Research 86, 1873–1887.

Burg, J.P., Iglesias, M., Laurent, P., Matte, P., Ribeiro, A., 1981. Variscan intracontinental deformation: The Coimbra–Cordona shear zone (SW Iberian Peninsula). Tectonophysics 78, 161–177.

Carey, S.W., 1955. The orocline concept in geotectonics. Proceedings of the Royal Society of Tasmania 89, 255–288.

De Sitter, L.U., 1965. The Hercynian Cantabrian orogen. Memoiria Geopaleontologia Università Ferrara 1, 211–225.

Fisher, R.A., 1953. Dispersion on a sphere. Proceedings of the Royal Society of London A 217, 295–305.

Hirt, A.M., Lowrie, W., Julivert, M., Arboleya, M.L., 1992. Paleomagnetic results in support of a model for the origin of the Asturian Arc. Tectonophysics 213, 321–339.

Hoffman, K.A., Day, R., 1978. Separation of multi-component NRM: A general method. Earth and Planetary Science Letters 40, 433–438.

Julivert, M., 1971. Décollement tectonics in the Hercynian Cordillera of NW Spain. American Journal of Science 270, 1–29.

Julivert, M., Arboleya, M.L., 1984. A geometrical and kinematical approach to the nappe structure in an arcuate foldbelt: The Cantabrian nappes (Hercynian chain, NW Spain). Journal of Structural Geology 6, 499–519.

Julivert, M., Arboleya, M.L., 1986. Areal balancing and estimate of areal reduction in a thin-skinned fold and thrust belt (Cantabrian Zone, northwest Spain). Journal of Structural Geology 8, 407–414.

Julivert, M., Marcos, A., 1973. Superimposed folding under flexural conditions in the Cantabrian Zone (Hercynian Cordillera, northwest Spain). American Journal of Science 273, 353–375.

Kirschvink, J.L., 1980. The least-squares line and plane and the analysis of paleomagnetic data. Geophysical Journal of the Royal Astronomical Society 62, 699–718.

Martinez-Garcia, E., 1991. Hercynian syn-orogenic and post-orogenic successions in the Cantabria and Palentian zones (NW Spain). Comparison with the western European occurrences. Giornale di Geologia 5311, 209–228.

Matte, P., Ribeiro, A., 1975. Forme et orientation de l'ellipsoide de déformation dans la viration hercynienne de Galicia: relation avec le plissement et hypothèses sur la génèse de l'arc ibéro-armoricain. Comptes Rendus Hebdomadaires des Séances de l'Académie des Sciences, Série D: Sciences Naturelles 280, 2825–2828.

Matte, P., 1986. Tectonics and plate tectonics model for the Variscan belt of Europe. Tectonophysics 126, 329–374.

Matte, P., 1991. Accretionary history and crustal evolution of the Variscan belt in western Europe. Tectonophysics 196, 309–337.

McCabe, C., Elmore, R.D., 1989. The occurrence and origin of Late Paleozoic remagnetization in the sedimentary rocks of North America. Reviews in Geophysics 27, 471–494.

McElhinny, M.W., 1964. Statistical significance of the fold test in paleomagnetism. Geophysical Journal of the Royal Astronomical Society 8, 338–340.

McFadden, P.L., Reid, A.B., 1982. Analysis of paleomagnetic inclination data. Geophysical Journal of the Royal Astronomical Society 69, 307–319.

Molina-Garza, R.S., Zijderveld, J.D.A., 1996. Paleomagnetism of Paleozoic strata, Brabant and Ardennes Massifs, Belgium: Implications of prefolding and postfolding Late Carboniferous secondary magnetizations for European polar wander. Journal of Geophysical Research 101, 15,799–15,818.

Nairn, A.E.M., Smithwick, M.E., 1976. Permian paleogeography and climatology. In: The Continental Permian in Central, West, and South Europe, NATO ASI Series. Series C: Mathematical and Physical Sciences, 22. D. Reidel Publishing Company, pp. 283–312.

Parés, J.M., Van der Voo, R., Stamatakos, J.A., Pérez-Estaún, A., 1994. Remagnetization and postfolding oroclinal rotations in the Cantabrian/Asturian Arc, northern Spain. Tectonics 13, 1461–1471.

Parés, J.M., Van der Voo, R., Stamatakos, J.A., 1996. Palaeomagnetism of Permian and Triassic red beds of NW Spain and implications for the tectonic evolution of the Austurian–Cantabria Arc. Geophysical Journal International 126, 893–901.

Pérez-Estaún, A., Bastida, F., Alonso, J.L., Marquinez, J., Aller, J., Alvarez-Marrón, J., Marcos, A., Pulgar, J.A., 1988. A thin-skinned tectonics model for an arcuate fold and thrust belt: The Cantabrian Zone (Variscan Armorican Arc). Tectonics 7, 517–537.

Pérez-Estaún, A., Bastida, F., Martinez-Catalan, J.R., Gutierrez, Marco J.C., Marcos, A., Pulgar, J.A. 1990. Chapter 2: Stratigraphy. In: Dallmeyer, R.D., Martinez-Garcia, E. (Eds.), Pre-Mesozoic Geology of Iberia. Springer-Verlag, Berlin, pp. 92–102.

Perroud, H., 1982. Relations paléomagnétisme et déformation: Exemple de la région de Cabo de Peñas (Espagne). Comptes rendus de l'Académie des sciences. Série II, Sciences de la terre et des planètes 294, 45–48.

Perroud, H., 1983. Paleomagnetism of Paleozoic rocks from the Cabo de Peñas, Asturia, Spain. Geophysical Journal of the Royal Astronomical Society 75, 201–215.

Perroud, H., 1985. Paléomagnétisme dans l'arc ibéro-armoricain et l'orogénèse Varisque en Europe occidentale. Ph.D. thesis, Univ. de Rennes I, Rennes, France.

Perroud, H., 1986. Paleomagnetic evidence for tectonic rotations in the Variscan Mountain Belt. Tectonics 5, 205–214.

Ponce de Leon, M., Choukroune, P., 1980. Shear zones in the Iberian Arc. Journal of Structural Geology 2, 63–68.

Ramsay, J.G., 1960. The deformation of early linear structures in areas of repeated folding. Journal of Geology 68, 75–93.

Ramsay, J.G., 1962. Interference patterns produced by the superposition of folds of "similar" type. Journal of Geology 60, 466–481.

Raven, J.G.M., Van der Pluijm, B.A., 1986. Metamorphic fluids and transtension in the Cantabria Mountains of northern Spain: an application of the conodont colour alteration index. Geology Magazine 123, 673–681.

Reijers, T.J.A., 1980. Sedimentary mechanisms in Spanish Devonian Carbonates. Geologie en Mijnbouw 59, 87–96.

Reijers, T.J.A., 1985. Devonian basin-fill histories of the Spanish Cantabrian Mountains and the Belgian Ardennes; a comparison. Geologie en Mijnbouw 64, 41–62.

Ries, A.C., Shackleton, R.M., 1976. Pattern of strain variation in arcuate fold belts. Philosophical Transactions of the Royal Society of London 283, 281–288.

Ries, A.C., Richardson, A., Shackleton, R.M., 1980. Rotation of the Iberian arc: Paleomagnetic results from north Spain. Earth Planetary Science Letters 50, 301–310.

Setiabudidaya, D.J., Piper, D.A., Shaw, J., 1994. Paleomagnetism of the (Early Devonian) Lower Old Red sandstones of south Wales: Implications to Variscan overprinting and differential rotations. Tectonophysics 231, 257–280.

Stewart, S.A., 1995. Paleomagnetic analysis of fold kinematics and implications for geological models of the Cantabrian/Asturian Arc, north Spain. Journal of Geophysical Research 100, 20,079–20,094.

Thominski, H.P., Wohlenberg, J., Bleil, U., 1993. The remagnetization of Devono-Carboniferous sediments from the Ardennes–Rhenish Massif, Germany. Tectonophysics 225, 411–431.

Van der Voo, R., 1993. Paleomagnetism of the Atlantic, Tethys and Iapetus Oceans. Cambridge University Press, New York.

Van der Voo, R., Stamatakos, J.A., Parés, J.M., 1997. Kinematic constraints on thrust-belt curvature from syndeformational magnetizations in the Lagos del Valle Syncline in the Cantabrian Arc, Spain. Journal of Geophysical Research 102, 10,105–10,120.

Ziegler, P.A., 1982. Geological Atlas of Western and Central Europe. Elsevier, Amsterdam.

Zijderveld, J.D.A. 1967. AC demagnetization of rocks: Analysis of results. In: Collison, D.W., Runcorn, S.K., Creer, K.M. (Eds.), Methods in Paleomagnetism. Elsevier, New York, pp. 254–286.